Influence of pulse frequency on microstructure and mechanical properties of Al-Ti-V-Cu-N coatings deposited by HIPIMS

MEI, Haijuan, DING, Ji Cheng, XIAO, Xiaolan, LUO, Quanshun <http://orcid.org/0000-0003-4102-2129>, WANG, Rui, ZHANG, Quan, GONG, Weiping and WANG, Qimin

Influence of pulse frequency on microstructure and mechanical properties of Al-Ti-V-Cu-N coatings deposited by HIPIMS

Haijuan Mei [a,b,*], Ji Cheng Ding [c], Xiaolan Xiao [b], Quanshun Luo [d],
Rui Wang [b], Quan Zhang [b], Weiping Gong [a], Qimin Wang [b,*]

[a] *Guangdong Provincial Key Laboratory of Electronic Functional Materials and Devices, Huizhou University, Huizhou, China*

[b] *School of Electromechanical Engineering, Guangdong University of Technology, Guangzhou, China*

[c] *School of Convergence Science, Pusan National University, Busan 609-735, South Korea*

[d] *Materials and Engineering Research Institute, Sheffield Hallam University, Sheffield, S1 1WB, UK*

* Corresponding author: haijuanmei@hzu.edu.cn (Haijuan Mei),
qmwang@gdut.edu.cn (Qimin Wang).

ABSTRACT

As an important parameter of HIPIMS, pulse frequency has significant influence on the microstructure and mechanical properties of the deposited coatings, especially for the multi-component coatings deposited by using a spliced target with different metal sputtering yields. In this study, a single $Al_{67}Ti_{33}$-V-Cu spliced target was designed to prepare Al-Ti-V-Cu-N coatings by using high power impulse magnetron sputtering (HIPIMS). The results showed that the peak target current density decreased from 0.75 to 0.24 $A \cdot cm^{-2}$ as the pulse frequency increased, along with the microstructure transferred from dense structure to coarse column structure. The pulse frequency has significant influence on chemical compositions of Al-Ti-V-Cu-N coatings, especially for Cu content increasing from 6.2 to 11.7 at.%. All the coatings exhibited a single solid-solution phase of Ti-Al-V-N, and the preferred orientation changed from (111) to (220) when the pulse frequency increased above 200 Hz. The decrease in peak target current density at high pulse frequencies resulted in a sharp decrease in the coating hardness from 35.2 to 16.4 GPa, whereas the relaxation of compressive residual stress contributed to an improvement in adhesion strength from 43.3 to 79.6 N.

Keywords: Al-Ti-V-Cu-N; Pulse frequency; Microstructure; Mechanical properties.

1. Introduction

Hard coatings have been widely applied for high-speed machining and cutting, which significantly improved the cutting life of coated tools. Among which, ternary TiAlN coatings were widely investigated due to excellent properties, including high hardness [1], oxidation resistance [2], corrosion resistance [3], and wear resistance [4]. Recently, the addition of vanadium has been reported to further improve the wear resistant of $Ti_{1-x}Al_xN$ based hard coatings. Due to the lubrication oxides of Magnéli phases (e.g. V_2O_5) formed at elevated temperatures, Ti-Al-V-N coatings has been used as a potential candidate for anti-wear coatings [5, 6]. However, the addition of V in TiAlN coatings led to an earlier formation of rutile TiO_2 and degraded the oxidation resistance of Ti-Al-V-N coatings [7]. In addition, the wear resistance of Ti-Al-V-N coatings deteriorated with the increase of V content due to the reduced resistance to oxidation at 500 °C [8]. It is well known that the hard coatings alloyed with some soft metal phases (e.g. Cu, Ag) to form

nanocomposite structures could further improve the toughness and hardness [9] and obtain even lower friction coefficient [10–12]. For example, the addition of Cu in AlTiN coatings could significantly improve the coated tool life, which would due to the combination of self-lubricating effect and reduced thermal conductivity [13]. As is known to all, multicomponent coatings often possess various outstanding comprehensive properties such as high hardness, excellent wear resistance, good good ductility [14, 15]. Thus, it's considered that the comprehensive performance of Ti-Al-V-N coatings could be further enhanced by alloying with Cu.

To obtain superior coating performances, an advanced PVD technique, namely high power impulse magnetron sputtering (HIPIMS), has been widely applied for the deposition of hard coatings. In HIPIMS plasma, a highly ionized flux with high ion energy could be achieved by loading a high peak power densities to the target with a low duty cycle of less than 10% and a low pulse frequency less than 1 kHz [16]. As an important parameter of HIPIMS pulse, the pulse frequency has significant influence on the microstructure evolution and mechanical properties of the deposited coatings. For example, Samuelsson et al. [17] have studied the effect of pulse frequency on the deposition of ZrB_2 coatings. Due to the degree of ionization increased, the residual stress changed from tensile to compressive when the pulse frequency decreased from 900 to 300 Hz. Nedfors et al. [18] have investigated the effect of pulse frequency, ranging from 200 to 1000 Hz, on the residual stress and mechanical properties of TiB_2 coatings. Due to the ion-flux to the substrate increased at low pulse frequencies, the highest hardness of 49 GPa and compressive residual stress of 3.8 GPa achieved for the coating deposited at 200 Hz. Dai et al. [19] have explored the influence of pulse frequency on the deposition of diamond-like carbon coatings with AlCrSi co-doping. The high pulse frequency (400 Hz) effectively prevented the poisoning of metal target and decreased the arcing events, resulting in a smooth surface without macro-droplets. However, the effect of pulse frequency on the deposition of Al-Ti-V-Cu-N coatings has not been reported, especially for the multi-component coatings deposited by using a spliced target with different metal sputtering yields.

The aim of this work was to investigate the influence of pulse frequency on the deposition and characteristics of Al-Ti-V-Cu-N coatings. The relationship between the pulse frequency and peak target current density, deposition rate, chemical composition, phase structure, residual stress and mechanical properties of Al-Ti-V-Cu-N coatings has been studied.

2. Experimental

2.1. Coating deposition

Al-Ti-V-Cu-N coatings were deposited on cemented carbide and 316L stainless steel substrates by HIPIMS using a rectangular $Al_{67}Ti_{33}$-V-Cu spliced target (99.9% purity, 69 mm × 443 mm), which was consist of two metal targets of Cu and V, and a $Al_{67}Ti_{33}$ alloy target. The calculated erosion area of the spliced target was 239.5 cm^2. In Fig. 1, a rotational substrate holder with a rotation speed of 3 rpm was fixed at the center of $Al_{67}Ti_{33}$-V spliced target, with a horizontal distance of 120 mm between the target and substrate holder. Before the deposition, all the cleaned and dried samples were installed on the rotational substrate holder. The vacuum chamber was pumped down to 5.0×10^{-3} Pa and heated up to 200 °C. After the substrates were etched by ion bombardment in pure Ar gas for 15 min, a thin inter-layer of CrN was first prepared by arc ion plating at a DC substrate bias of −120 V for 10 min. Al-Ti-V-Cu-N coatings were deposited by HIPIMS technique at a target power of 1.0 kW and a constant pulse length of 100 μs, whereas the pulse frequency varied from 160 to 500 Hz.

During the coating deposition, the target voltage and current were measured by a digital phosphor oscilloscope (Tektronix, 2002B) with a voltage probe and a current monitor, respectively. The formula of average target power P_a was shown as below:

$$P_a = f\int_0^{\tau} V(t)I(t)dt \quad (1)$$

where f and τ refer to the pulse frequency and pulse length, $V(t)$ and $I(t)$ refer to the target voltage

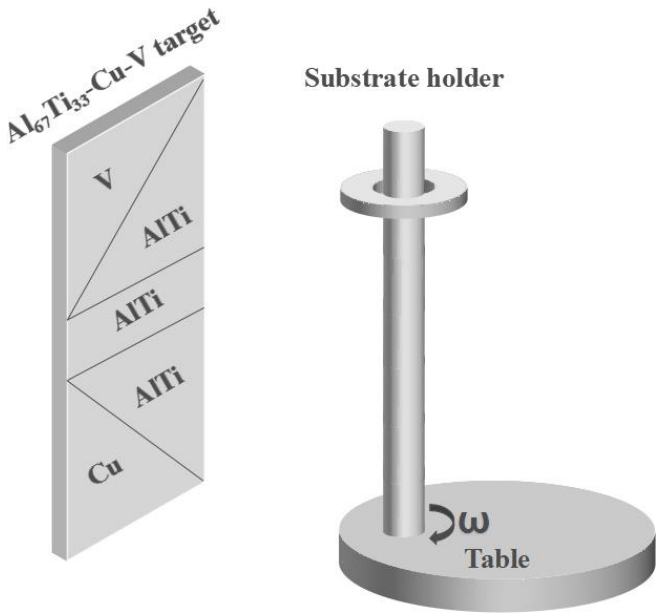

Fig. 1. Schematic diagram of the $Al_{67}Ti_{33}$-V-Cu spliced target and substrate position.

Table 1 Deposition parameters of Al-Ti-V-Cu-N coatings deposited by HIPIMS.

Parameters	Values
Base pressure (Pa)	5.0×10^{-3}
Working pressure (Pa)	0.6
N_2 /Ar flow rate (sccm)	10 / 40
Working temperature (°C)	200
Bias voltage (V)	–100
Target power (kW)	1.0
Pulse length (μs)	100
Pulse frequency (Hz)	160, 200, 300, 400, 500
Duty cycle	1.6%, 2%, 3%, 4%, 5%
Deposition time (min)	180

and current, respectively. The deposition time was kept constant at 180 min, and the detail parameters of deposition were listed in Table 1.

2.2. Coating characterization

The surface and cross-section morphologies of the coatings were characterized by a field emission scanning electron microscopy (FE-SEM, Nano430), operating at an accelerating voltage of 10 kV. Then the deposition rates were calculated according to the coating thickness observed from the cross-sections. The chemical compositions were determined by energy-dispersive X-ray spectrum (EDX). The crystal structure of the coatings were analyzed by a X-ray diffraction (XRD, Bruker D8 Advance) with Cu K_α radiation operated at 40 kV and 40 mA. The instrument was carried out in the Bragg-Brentano mode at a scanning range of 10° – 90° with a step size of 0.02°. Then the preferred orientations were quantified by the texture coefficient formula [20]:

$$T_{(hkl)}=\frac{I_{(hkl)}/I_{0(hkl)}}{\frac{1}{n}\sum_{n=1}^{n} I_{(hkl)}/I_{0(hkl)}} \quad (2)$$

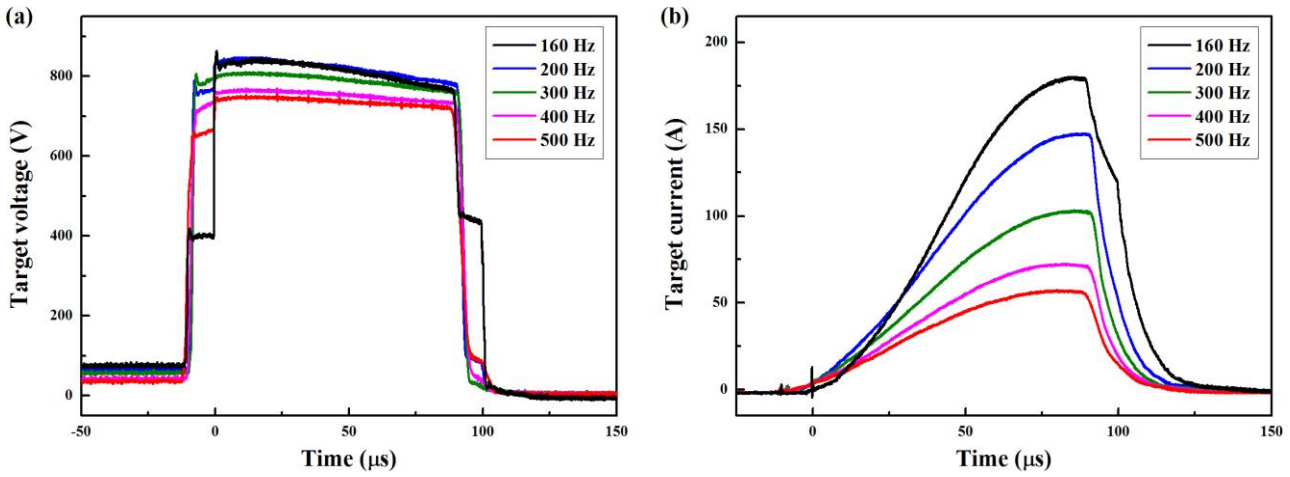

Fig. 2. The electrical characteristics of (a) target voltage and (b) target current of the $Al_{67}Ti_{33}$-V-Cu spliced target at various pulse frequencies.

where $I_{(hkl)}$ and $I_{0(hkl)}$ refer to the intensity of the measured (*hkl*) peak in the coatings and the relative standard intensity of TiN powder (JCPDS 38-1420) respectively, and *n* is the number of reflections considered. Selected sample was further characterized the chemical bonding state of the coating by X-ray photoelectron spectroscopy (XPS, Escalab 250Xi). Before the measurement, the coating surface was sputter etched by Ar^+ (3 keV) ion bombardment for 120 s to remove the surface contamination.

The residual stress of the coatings were determined on stainless steel substrates by a film stress tester (FST-1000, Supro Instruments) based on the substrate curvature method [21]. The coating hardness and elastic modulus were measured on cemented carbide substrates by nanoindenter (NHT^2, CSM). At least five indentation tests were carried out for each sample at a maximum applying load of 10 mN. The adhesion strength of the coatings were examined by a scratch tester (RST, CSM) at a maximum load of 80 N and a scratch length of 3 mm.

3. Results and discussion

3.1. Discharge characteristic and deposition rate

Fig. 2 shows the characteristics of HIPIMS discharge of $Al_{67}Ti_{33}$-V-Cu spliced target at various pulse frequencies. As shown in Fig. 2(a), all the pulse lengths kept constant at 100 μs with the pulse frequency ranging from 160 to 500 Hz, and all the target voltages exhibited a rectangular pulse shape. The peak target voltage increased from 755 to 864 V when the pulse frequency decreased from 500 to 160 Hz. The time -dependent target current was plotted in Fig. 2(b), the target current first increased sharply to a maximum value, and then reached a stable status for a short time. When the pulse frequency decreased, similar trends observed in the peak target current that increased drastically from 58 to 180 A. At the lowest pulse frequency of 160 Hz, the shape of target current exhibited a fluctuating curve at the end of pulse, indicating that the spliced target discharge was unstable at a low pulse frequency below 160 Hz.

Fig. 3(a) presents the peak target current density as a function of pulse frequency. The peak target current density decreased linearly from 0.75 to 0.24 $A \cdot cm^{-2}$ when the pulse frequency increased. It was reported that a high peak target current resulted in an increase of ionization rate and plasma density [22, 23]. Thus, it can be inferred that the ionization rate of spliced target increased with the decrease of pulse frequency. Moreover, the average target power P_a at various pulse frequencies were calculated by using Eq. (1), which was also plotted in Fig. 3(a). It was worth noting that the average target power P_a increased linearly from 1.24 kW to a maximum value of 1.38 kW when pulse frequency increased from 160 to 300 Hz, and then decreased to 1.27 kW at 500 Hz. The variation in average target power P_a would be directly related to the decrease of target voltage and current at high pulse frequencies. As shown in Fig. 3(b), the deposition rate increased linearly from 4.1 to 5.9 nm/min with increasing the pulse frequency from 160 to 300 Hz. This

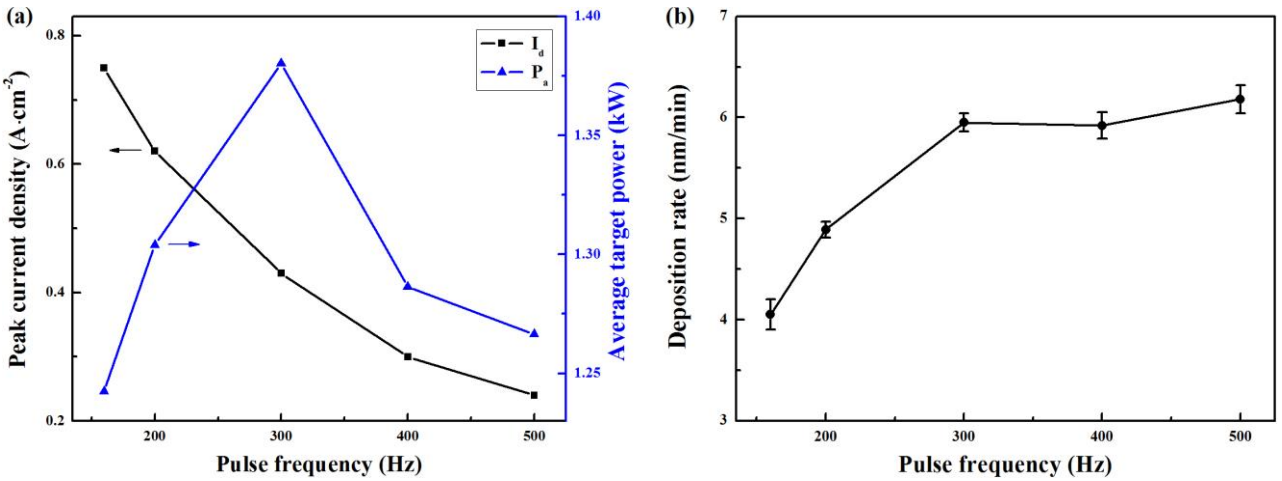

Fig. 3. (a) The peak current density and average target power, and (b) deposition rates of the coatings at various pulse frequencies.

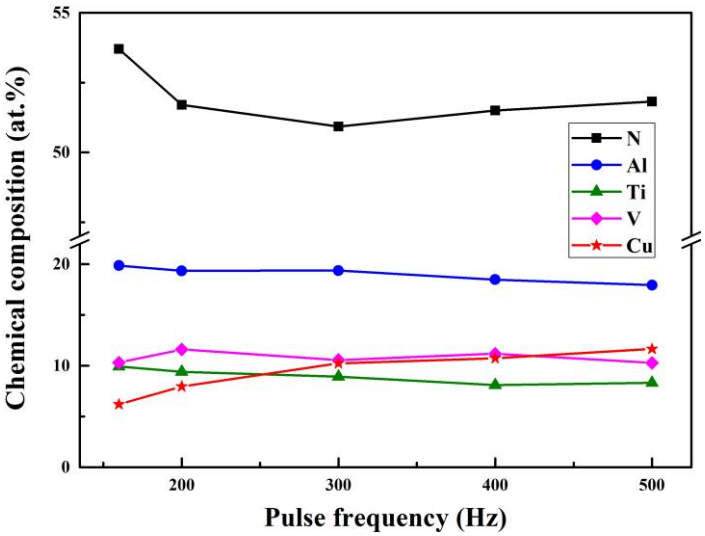

Fig. 4. Chemical compositions of Al-Ti-V-Cu-N coatings deposited at various pulse frequencies.

demonstrated that the higher deposition rates achieved at higher average target powers. However, when the pulse frequency further increased to 500 Hz, the deposition rate increased up to 6.2 nm/min, which would be related to the sharp decrease of peak target current density. The back attraction effects at target surface reduced at a low ionization rate, which led to more metal ions and atoms flied toward the substrates, contributing to an increase in deposition rate [24]. Additionally, due to the weakening of ion bombardment at high pulse frequencies, the reflection or desorption of atoms and ions at the substrate surface decreased, which would also contribute to the increase of deposition rate [25].

3.2. Chemical composition and microstructure

Fig. 4 illustrates the chemical compositions of Al-Ti-V-Cu-N coatings deposited at various pulse frequencies. With increasing the pulse frequency, N content initially decreased and then remained at ~51.5 at.%. The N/(Al+Ti+V) atomic ratios were in the range from 1.28 to 1.42, indicating that a relatively high N_2/Ar gas ratios of 1:4 resulted in the over-stoichiometric of N element in Al-Ti-V-Cu-N coatings. Moreover, the calculated Al/Ti atomic ratios were found in the range of 2.0 to 2.3, which was slightly higher than the original contents in $Al_{67}Ti_{33}$ alloy target. It demonstrated that a higher sputtering yield achieved for Al element than that of Ti element sputtered from the alloy target [26]. Due to the different mass of the sputtered elements of Al and Ti, leading to the scattering and variation of gas phase during the metal atoms transported from the target to substrate [27]. In addition, the re-sputtering by Ti ions would occur due to the higher ionization rate of Ti than Al, which led to a decrease in Ti species deposited on the substrate surface

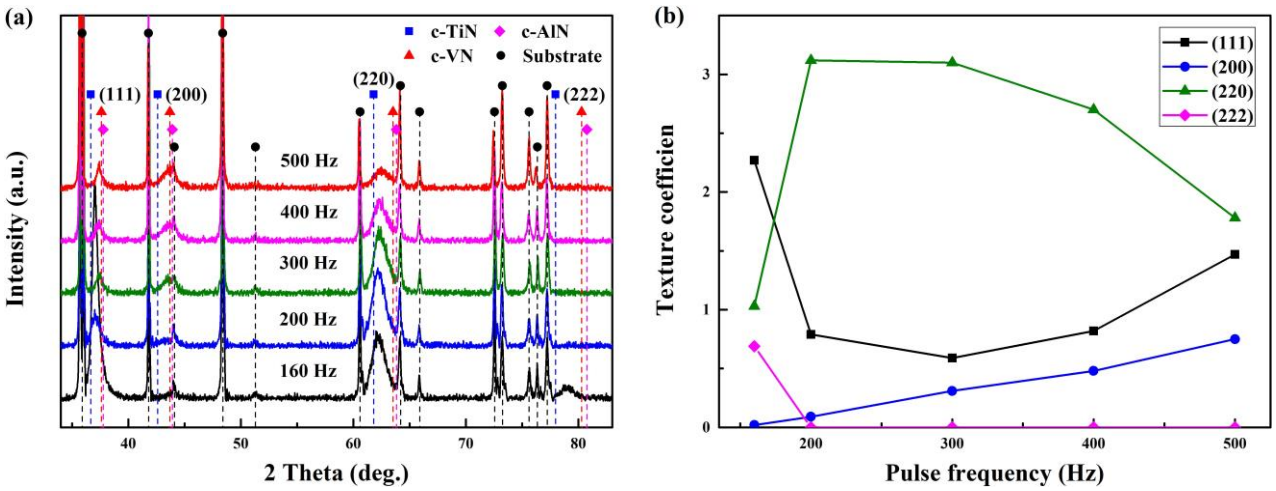

Fig. 5. (a) X-ray diffractograms and (b) texture coefficients of Al-Ti-V-Cu-N coatings deposited at various pulse frequencies.

[28]. When the pulse frequency increased from 160 to 500 Hz, V content was kept in a small range of 10.3 to 11.6 at.%, while Cu content increased gradually from 6.2 to 11.7 at.%. This phenomenon would be due to the decrease of peak target current density at high pulse frequencies, leading to a decrease in ionization rate of the metal atoms which reacted easily with nitrogen. Meanwhile, Cu element has much higher sputtering yield and lower ions/atoms ratio in the plasma [29], contributing to an increase in Cu content at higher pulse frequencies. Thus, the calculated stoichiometric ratio of the coatings changed from $Al_{0.20}Ti_{0.10}V_{0.10}Cu_{0.06}N_{0.54}$ at 160 Hz to $Al_{0.18}Ti_{0.08}V_{0.10}Cu_{0.12}N_{0.52}$ at 500 Hz. This implied that pulse frequency has significant influence on the chemical compositions of $Al_{67}Ti_{33}$-V-Cu spliced target, especially for Cu element.

Fig. 5(a) shows the X-ray diffractograms of Al-Ti-V-Cu-N coatings deposited at various pulse frequencies. As compared with the standard peaks of c-TiN (JCPDS 38-1420), c-AlN (JCPDS 25-1495), and c-VN (JCPDS 35-0768) as inserted in Fig. 5(a), all the diffraction peaks of the coatings were centered between the standard peaks. It implied that all the coatings exhibited a cubic-type B1 structure with (111), (200), (220) and (222) crystal planes, corresponding to a solid-solution phase of Ti-Al-V-N. Due to the similar atomic radius of Al and V, the solid solution phase of Ti-Al-V-N was formed by the incorporation of V in face-centered-cubic (FCC) TiAlN lattice [6]. Although a diffraction peak at ~43.3° closed to the (111) plane of Cu phase (JCPDS 85-1326), but no other diffraction peaks of Cu phase could be identified in the X-ray diffractograms, indicating that Cu atoms distributed within the Ti-Al-V-N lattice or in an amorphous state. When the pulse frequency increased, the diffraction intensity of nitride coatings decreased, indicating that a decrease in crystallinity. In addition, all the diffraction peaks shifted toward higher diffraction angles with increasing the pulse frequency, implying that a decrease in lattice parameters. To clarify this point, the lattice parameters and strains of Al-Ti-V-Cu-N coatings were calculated by using Gaussian fittings [30], as listed in Table 2. As the pulse frequency increased from 160 to 500 Hz, the lattice parameters decreased from 4.20 to 4.17 Å. This phenomenon could be due to the relaxation of residual stress induced by the reduced ion bombardment at high pulse frequencies. Meanwhile, the increased Cu content at high pulse frequencies would also contribute to the decrease of lattice parameters. It was found that the Cu atoms escaped from the Mo-N lattices when the Cu content increased above 7 at.%, resulting in the resultant lattice shrink [31].

The intensity of preferred orientation was quantified by texture coefficient $T_{(hkl)}$, which can be calculated by using Eq. (2). As shown in Fig. 5(b), it was found that the pulse frequency has a significant influence on the texture coefficient of Al-Ti-V-Cu-N coatings. At a low pulse frequency of 160 Hz, the coating exhibited a strong (111) preferred orientation with a high texture coefficient of 2.27, which demonstrated that the strong ion bombardment enhanced the (111) texture. Similar results were observed in AlTiN coatings deposited by HIPIMS that the (111) preferred orientation

Table 2 Lattice parameters and strains of Al-Ti-V-Cu-N coatings at various pulse frequencies.

Planes	Lattice parameters a_0 (Å)					Strains ε (%)				
	1.6%	2%	3%	4%	5%	1.6%	2%	3%	4%	5%
(111)	4.20	4.20	4.16	4.16	4.16	0.74	1.07	0.75	0.65	0.60
(200)	4.19	4.19	4.16	4.16	4.16	1.29	1.29	1.24	1.30	1.28
(220)	4.22	4.21	4.21	4.21	4.20	1.06	1.01	0.90	0.98	1.01
(222)	4.20	—	—	—	—	0.68	—	—	—	—
Mean	4.20	4.20	4.18	4.18	4.17	0.94	1.12	0.96	0.98	0.96
Stdev	0.01	0.01	0.03	0.03	0.02	0.29	0.15	0.25	0.33	0.34

induced by the strong ion bombardment [32]. When the pulse frequency increased to 200 Hz, the texture coefficient of (111) plane decreased sharply to 0.79, while the (220) plane achieved the highest texture coefficient of 3.12. Thus, the preferred orientation of the coatings has changed from (111) to (220) at high pulse frequencies above 200 Hz. In addition, the (222) diffraction peak disappeared and a weak (200) plane with a low texture coefficient of 0.09 appeared. According to thermodynamic model [33], as for the transition metal nitrides with B1-NaCl structure, (111) plane with the lowest strain energy can be expected when the strain energy was dominant, while (200) plane with the lowest surface energy can be predicted when the surface energy was dominant. Thus, the preferred orientation of (220) plane observed for Al-Ti-V-Cu-N coatings at high pulse frequencies cannot be explained by above surface energy or strain energy model. According to growth kinetic model [34], the (111) plane is more close-packed of NaCl structure, while the (220) plane is the most open channeling direction. Thus, (220) plane have a higher probability of survival than (111) plane due to anisotropy of collision effect [14]. In addition, another picostructural model presented by Perry et al. [35] that the texture of TiN coatings could be affected by the formed lattice defects. As for the over-stoichiometric TiN coatings, the additional nitrogen was incorporated as dumb-bell pairs in the second nearest neighbor tetrahedral sites, which resulted in the preferred orientation of (200) or (220) plane. Similarly, the over-stoichiometric Al-Ti-V-Cu-N coatings favored a strong (220) preferred orientation with the highest lattice strain of 1.12% at 200 Hz. When pulse frequency increased to 500 Hz, the texture coefficient of (220) plane decreased to 1.78, while that of (111) and (200) planes reached 1.47 and 0.75, respectively, indicating no obvious preferred orientation. In this study, by applying increased pulse frequency, the additional energy delivered on the coating surface by ions bombardment decreased. Thus, these variations in preferred orientation of Al-Ti-V-Cu-N coatings was related to the combination effect of surface energy, adatom mobility and ion bombardment.

Fig. 6 shows the fitted XPS spectra of Al 2p, Ti 2p, V $2p_{3/2}$, Cu $2p_{3/2}$ and N 1s of the Al-Ti-V-Cu-N coating deposited at 300 Hz. As depicted in Fig. 6(a), the Al 2p spectra could be fitted into two sub-peaks: a major peak at 73.8 eV and a weak peak at 75.1 eV, corresponding to TiAlVN and Al_2O_3, respectively. A high binding energy of 77.3 eV was found in the Al $2p_{3/2}$ spectra, corresponding to the Al_2O_3. In Fig. 6(b), the asymmetric Ti 2p peak could be deconvoluted into four peaks, including the nitride peaks TiAlVN (Ti $2p_{3/2}$: 454.8 eV, Ti $2p_{1/2}$: 460.5 eV), and sub-stoichiometric peaks TiO_x (Ti $2p_{3/2}$: 456.6 eV, Ti $2p_{1/2}$: 462.3 eV) [36]. In Fig. 6(c), two peaks centered at 514.4 and 516.4 eV in the V $2p_{3/2}$ spectra can be corresponded to TiAlVN and V_2O_5 species, respectively. In Fig. 6(d), the Cu $2p_{3/2}$ spectra could be fitted into two peaks: a dominant peak at 932.6 eV and a weak peak at 933.9 eV, corresponding to metallic Cu and minor CuO, respectively. It indicated that the Cu atoms formed in metal state in the coatings. For the N 1s spectra in Fig. 6(e), a high binding energy centered at 399.0 eV can be corresponded to the contaminants such as organic or adsorbed N [37]. Whereas the major peak centered at 397.7 eV could be assigned to TiAlVN bonding, which demonstrated that the formation of Ti-Al-V-N solid

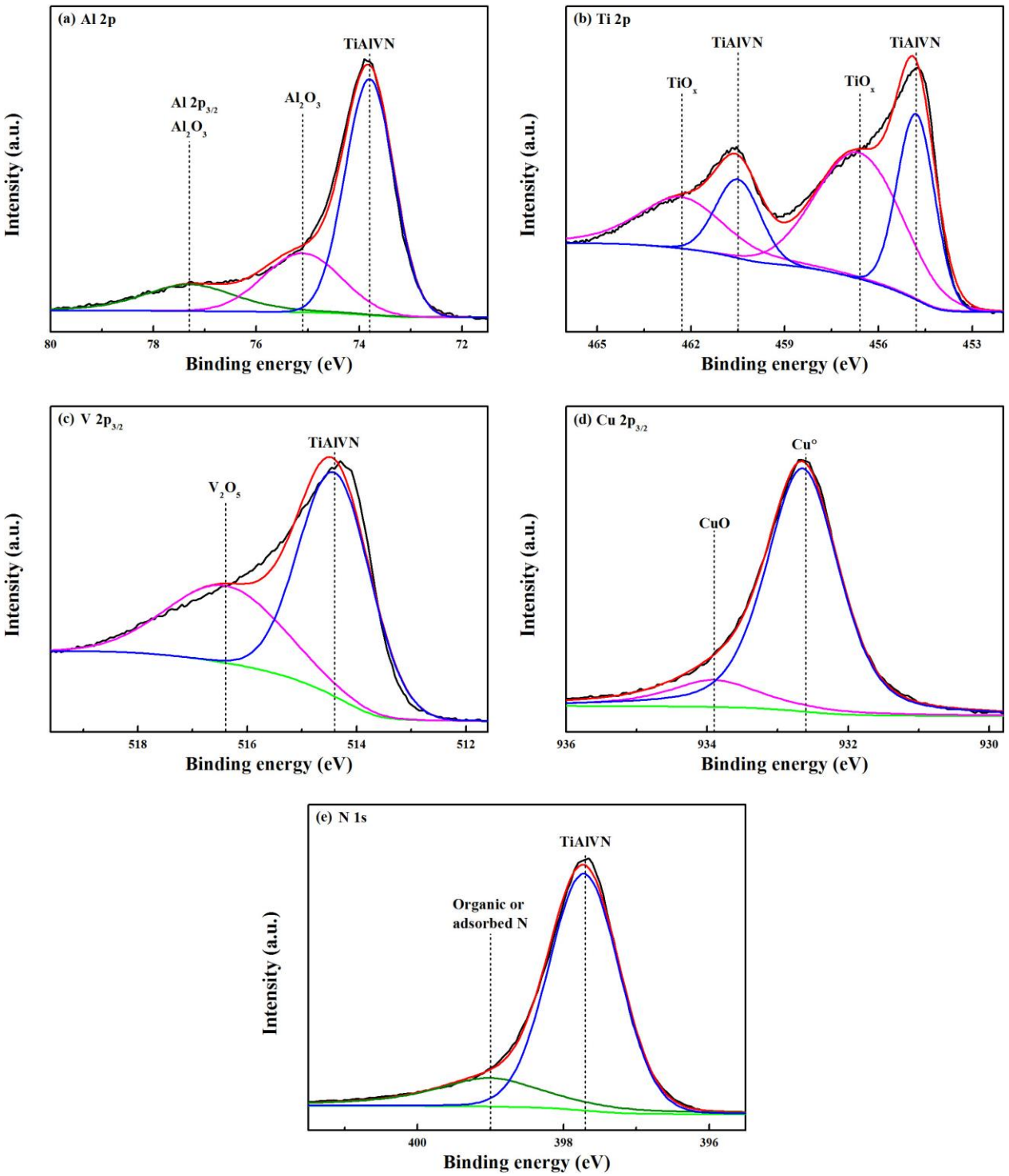

Fig. 6. Fitted XPS spectra of Al-Ti-V-Cu-N coating deposited at 300 Hz: (a) Al 2p, (b) Ti 2p, (c) V $2p_{3/2}$, (d) Cu $2p_{3/2}$, (e) N 1s.

solution phase in XRD.

Fig. 7 presents the surface morphologies of Al-Ti-V-Cu-N coatings deposited at various pulse frequencies. In Fig. 7(a)–(b), the coatings exhibited relatively smooth surfaces with few micro-particles at low pulse frequencies. Similar results were also found in TiN coatings deposited by HIPIMS that an increased ion bombardment led to a smooth surface at low duty cycles [38]. Moreover, the individual plate-like patterns could be clearly identified on the coating surfaces, which similar to the morphology of polished WC-Co substrate that used for the coating deposition. It would be due to the effect of strong ion bombardment and etching on growing coating surfaces, leading to obvious template growth effect. As the pulse frequency increased above 300 Hz, the

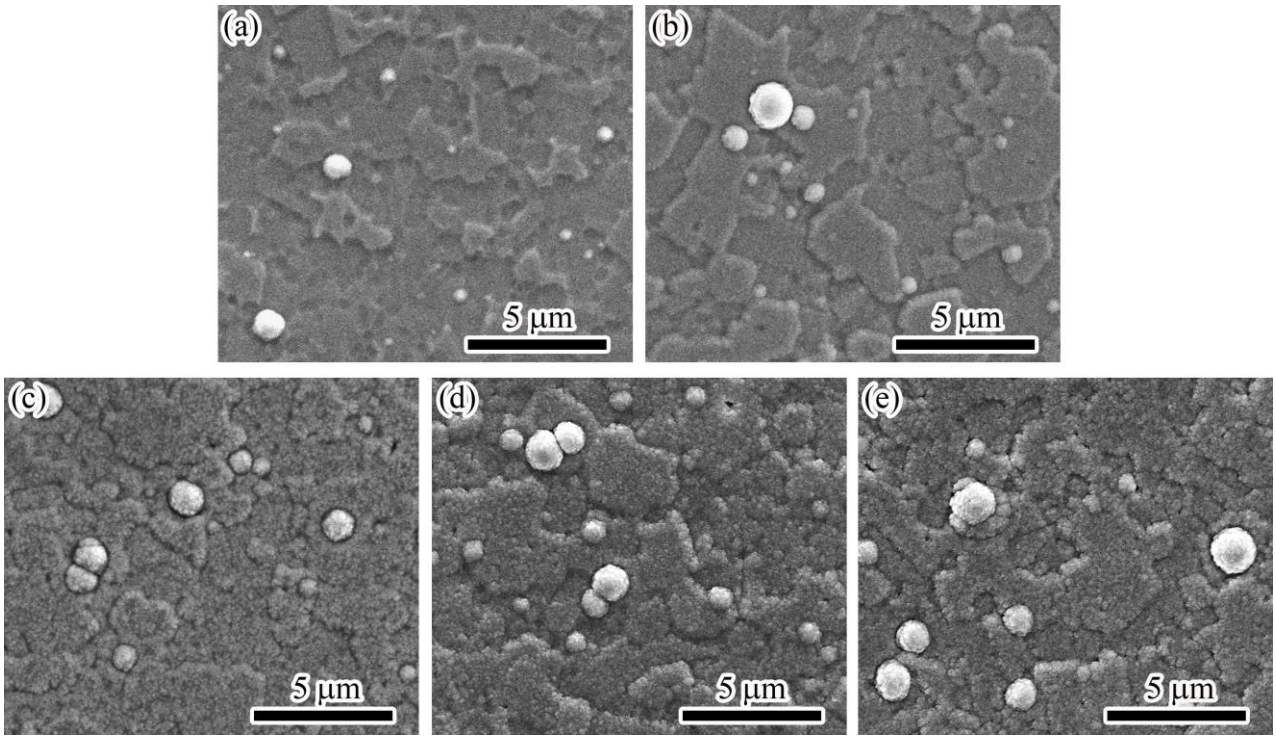

Fig. 7. Surface morphologies of Al-Ti-V-Cu-N coatings deposited at various pulse frequencies: (a) 160 Hz, (b) 200 Hz, (c) 300 Hz, (d) 400 Hz, (e) 500 Hz.

coating surfaces exhibited nanoscale granular structure, which would be corresponded to the top of columnar structure. When the pulse frequency increased, much more and larger micro-particles formed on the coating surfaces, implying that much rougher surfaces formed at higher pulse frequencies. Due to the peak target current density decreased at high pulse frequencies, the surface adatom energy and mobility induced by ion bombardment decreased, and reduced the grain boundary migration, resulting in the increase of the granular size and columns growth.

Fig. 8 displays the corresponding cross-sectional morphologies of Al-Ti-V-Cu-N coatings. Due to a dense CrN interlayer with a thickness of ~400 nm first prepared by arc ion plating, bi-layer structure can be clearly identified in the cross-sectionals of all coatings. No obvious grow defects could be observed in the interfaces, implying that a good adhesion interface achieved between Al-Ti-V-Cu-N coatings and the substrates. As shown in Fig. 8(a)–(b), Al-Ti-V-Cu-N coatings exhibited a dense and fine column structure at low pulse frequencies, which can be corresponded to II-type structure in Thornton model [39]. This dense column structure could be attribute to the effect of intense ion bombardment induced by the high peak target current density. However, when the pulse frequency increased above 300 Hz, the coatings exhibited a typical T-type structure with coarse columnar grains. This implied that the microstructure of Al-Ti-V-Cu-N coatings transferred from II-type to T-type structure with increasing the pulse frequency. Similar T-type and II-type structures were observed in TiAlN/VN coatings when the substrate bias voltage increased [40].

3.3. Mechanical properties

Fig. 9 shows the residual stress of Al-Ti-V-Cu-N coatings as a function of pulse frequency. All the coatings presented high compressive residual stress, especially for the coatings deposited at low pulse frequencies. When the pulse frequency increased from 160 to 300 Hz, the compressive residual stress decreased sharply from 5.6 to 2.3 GPa, then decreased slightly to 1.6 GPa at 500 Hz. Such a decrease in residual stress could be associated with two simultaneous effects. First, the relaxation of residual stress would be mainly due to the reduced ions bombardment effect induced by low peak current densities. It was found that the formation of sharp interfaces induced by high ion bombardment, which led to an increase in defect concentration and hence increased the compressive residual stress [41]. Second, the reduced residual stress would be related to the

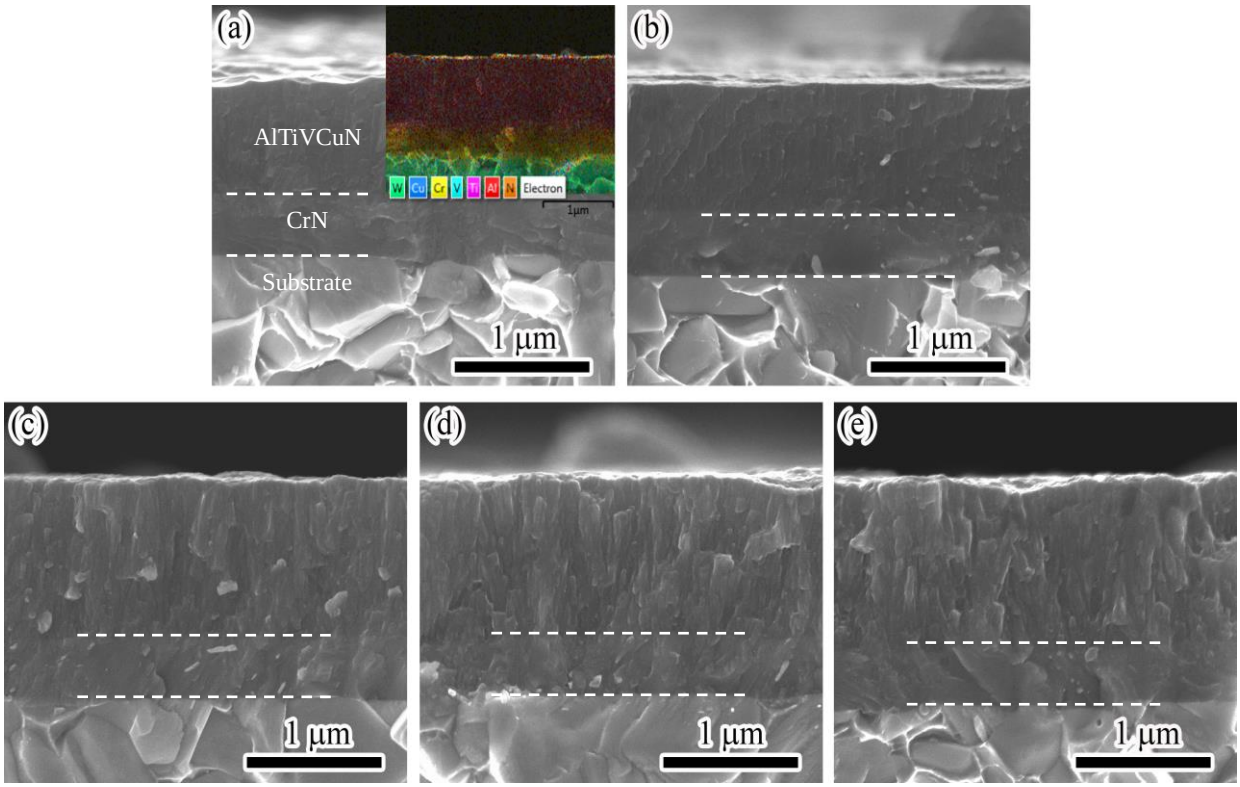

Fig. 8. Cross-sectional morphologies of Al-Ti-V-Cu-N coatings deposited at various pulse frequencies: (a) 160 Hz, (b) 200 Hz, (c) 300 Hz, (d) 400 Hz, (e) 500 Hz. Inset is the corresponding elemental mapping of the cross-section.

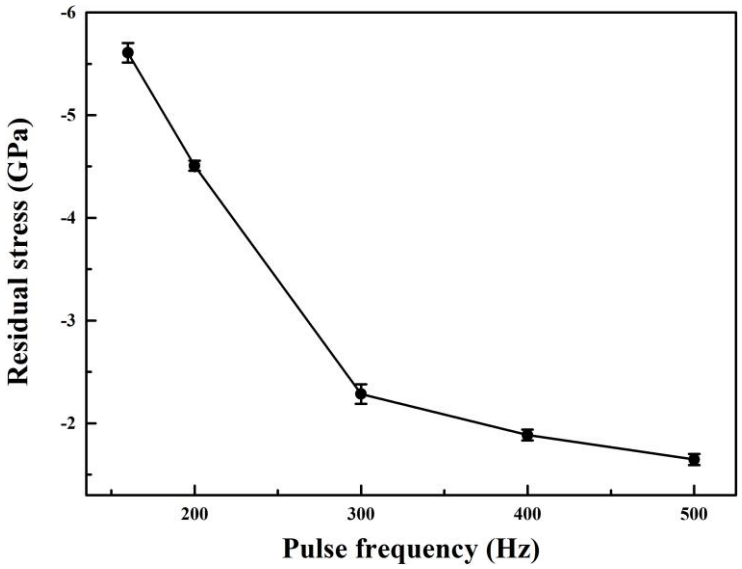

Fig. 9. Residual stress of Al-Ti-V-Cu-N coatings as a function of pulse frequency.

increase of Cu content in Al-Ti-V-Cu-N coatings at high pulse frequencies. Similar results were found in MoN coatings that the residual stress could be released by the presence of a ductile copper phase [42].

Fig. 10 displays the hardness and elastic modulus of Al-Ti-V-Cu-N coatings as a function of pulse frequency. It can be seen that the pulse frequency has a significant influence on the hardness and elastic modulus, which decreased sharply from 35.2 to 16.4 GPa and 461.1 to 348.6 GPa, respectively. It is well known that the hardness and elastic modulus of the coatings can be correlated to the variations of microstructure, residual stress and chemical composition. As discussed above, with increasing the pulse frequency, the ion bombardment effect reduced and the microstructure became coarser, which led to the decrease of coating hardness [43]. Meanwhile, the relaxation of

compressive residual stress and increased Cu content also resulted in the decrease of hardness and elastic modulus [44]. In addition, it was reported that the H^3/E^{*2} ratio could be used to predict the resistance against plastic deformation [45]. As same as the variation trend of hardness, the H^3/E^{*2} ratio decreased sharply from 0.18 to 0.03 when the pulse frequency increased from 160 to 500 Hz.

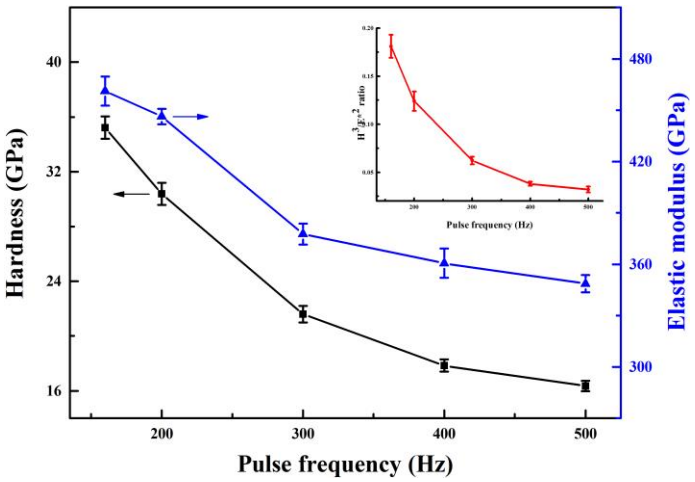

Fig. 10. Hardness and elastic modulus of the coatings as a function of pulse frequency. Inset is the corresponding H^3/E^{*2} ratio.

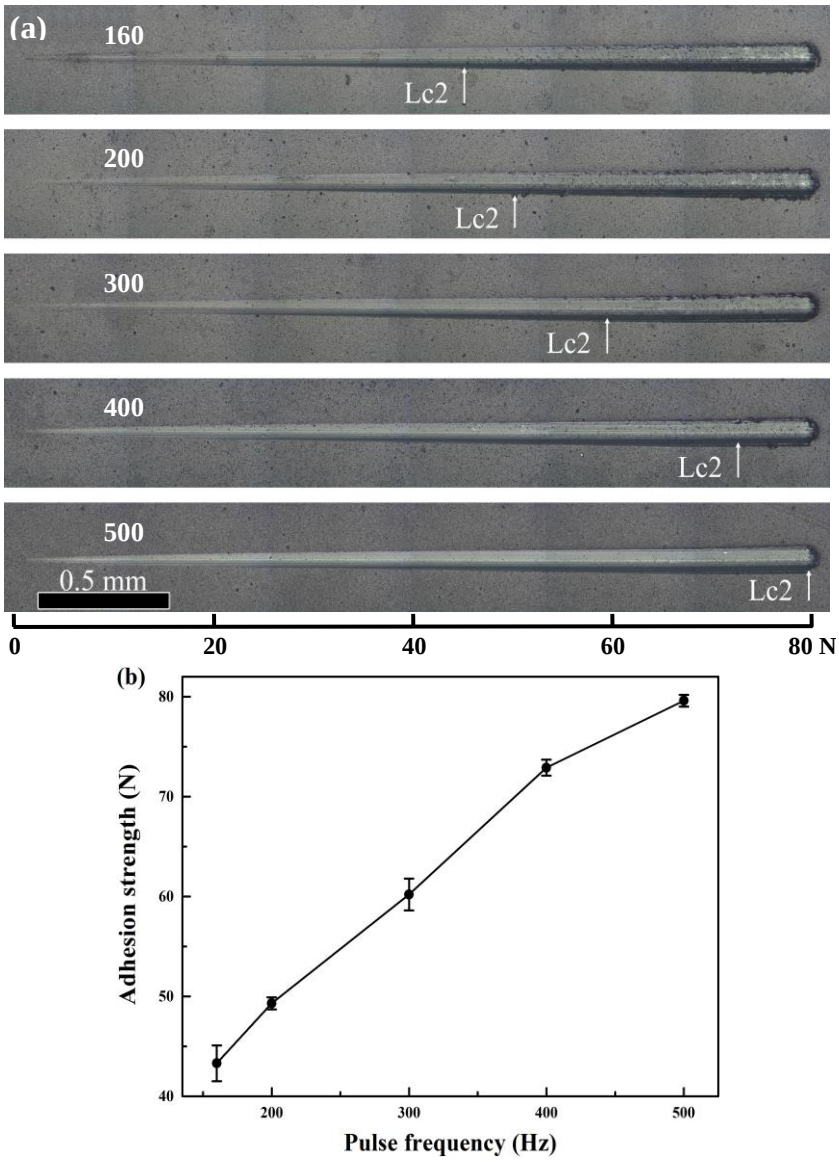

Fig. 11. (a) Scratch track morphologies and (b) adhesion strengths of Al-Ti-V-Cu-N coatings deposited at various pulse frequencies.

The adhesion strength of Al-Ti-V-Cu-N coatings were evaluated according to the morphologies of scratch tracks, which were observed by an optical microscope (OM). The full-length scratch track morphologies of the coatings deposited at various pulse frequencies were presented in Fig. 11(a). No obvious delamination was observed in the scratch tracks, implying that all coatings exhibited good adhesion with the WC-Co substrates due to the adhesion layer of CrN, which was in consistent with the dense coating/substrate interfaces observed in Fig. 8. Especially for the coating deposited at high pulse frequency of 500 Hz, only few edge chippings were found until the scratch load reaching a maximum value of 80 N, implying that an excellent adhesion strength was achieved. Fig. 11(b) shows the adhesion strength of Al-Ti-V-Cu-N coatings as a function of pulse frequency. It can be clearly seen that the adhesion strength increased linearly from 43.3 to 79.6 N when the pulse frequency increased from 160 to 500 Hz. The excellent adhesion strength would be benefited from the combined effects of high H^3/E^{*2} ratio and appropriate compressive residual stress [46, 47]. In current work, the improvement of adhesion strength of Al-Ti-V-Cu-N coatings at high pulse frequencies would be mainly due to the relaxation of high compressive residual stress.

4. Conclusions

Al-Ti-V-Cu-N coatings were synthesized by HIPIMS with a single $Al_{67}Ti_{33}$-V-Cu spliced target, and the influence of pulse frequency on the microstructure, chemical composition, residual stress, mechanical properties of the coatings was investigated. All the coatings exhibited a FCC Ti-Al-V-N solid-solution phase, and the preferred orientation changed from (111) to (220) at high pulse frequencies above 200 Hz. The pulse frequency has significant influence on chemical compositions of the coatings, especially for the Cu element. The stoichiometric ratios of the coatings changed from $Al_{0.20}Ti_{0.10}V_{0.10}Cu_{0.06}N_{0.54}$ at 160 Hz to $Al_{0.18}Ti_{0.08}V_{0.10}Cu_{0.12}N_{0.52}$ at 500 Hz. When the pulse frequency increased, the ion bombardment effect reduced, which resulted in a sharp decrease in coating hardness from 35.2 to 16.4 GPa, along with the decrease of compressive residual stress from 5.6 to 1.6 GPa, while the adhesion strength increased linearly from 43.3 to 79.6 N.

Acknowledgements

The authors gratefully acknowledged the National Natural Science Foundation of China (Grant No. 51875109, 51672100), Natural Science Foundation of Guangdong Province (Grant No. 2018A030310546), Program for Innovative Research Team of Guangdong Province & Huizhou University (IRTHZU), the Middle-aged and Young Teachers' Basic Ability Promotion Project of Guangxi (Grant No. 2018KY0662), the Professorial and Doctoral Scientific Research Foundation of Huizhou University (Grant No. 2020JB010).

References

[1] J. Musil, H. Hrubý, Superhard nanocomposite $Ti_{1-x}Al_xN$ films prepared by magnetron sputtering, Thin Solid Films 365 (2000) 104–109. https://doi.org/10. 1016/S0040-6090(00)00653-2.

[2] Z.B. Qi, P. Sun, F.P. Zhu, Z.T. Wu, B. Lin, Z.C. Wang, D.L. Peng, C.H. Wu, Relationship between tribological properties and oxidation behavior of $Ti_{0.34}Al_{0.66}N$ coatings at elevated temperature up to 900°C, Surf. Coat. Technol. 231 (2013) 267–272. https://doi.org/10.1016/j.surfcoat.2012.02.017.

[3] S.H. Ahn, J.H. Yoo, Y.S. Choi, J.G. Kim, J.G. Han, Corrosion behavior of PVD-grown WC-$(Ti_{1-x}Al_x)N$ films in a 3.5% NaCl solution, Surf. Coat. Technol. 162 (2003) 212–221. https://doi.org/10.1016/S0257-8972(02)00519-4.

[4] J.D. Bressan, R. Hesse, E.M. Silva, Abrasive wear behavior of high speed steel and hard metal coated with TiAlN and TiCN, Wear 250 (2001) 561–568. https:// doi.org/10.1016/S0043-1648(01)00638-X.

[5] R. Franz, C. Mitterer, Vanadium containing self-adaptive low-friction hard coatings for high-temperature applications: A review, Surf. Coat. Technol. 228 (2013) 1–13. https://doi.org/10.1016/j.surfcoat.2013.04.034.

[6] K. Kutschej, P.H. Mayrhofer, M. Kathrein, P. Polcik, C. Mitterer, A new low-friction concept for $Ti_{1-x}Al_xN$ based coatings in high-temperature applications, Surf. Coat. Technol. 188–189 (2004) 358–363. https://doi.org/10. 1016/j.surfcoat.2004.08.022.

[7] Y.X. Xu, L. Chen, F. Pei, J.L. Yue, Y. Du, Thermal stability and oxidation resistance of V-alloyed TiAlN coatings, Ceram. Int. 44 (2018) 1705–1710. https: //doi.org/10.1016/j.ceramint.2017.10.100.

[8] M. Pfeiler, K. Kutschej, M. Penoy, C. Michotte, C. Mitterer, M. Kathrein, The effect of increasing V content on structure, mechanical and tribological properties of arc evaporated Ti-Al-V-N coatings, Int. J. Refract. Met. H. 27 (2009) 502–506. https://doi.org/10.1016/j.ijrmhm.2008.06.008.

[9] H.S. Myung, H.M. Lee, L.R. Shaginyan, J.G. Han, Microstructure and mechanical properties of Cu doped TiN

superhard nanocomposite coatings, Surf. Coat. Technol. 163 (2003) 591–596. https://doi.org/10.1016/S0257-8972(02)00 627-8.

[10] C.Q. Dang, J.L. Li, Y. Wang, Y.T. Yang, Y.X. Wang, J.M. Chen, Influence of Ag contents on structure and tribological properties of TiSiN-Ag nanocomposite coatings on Ti-6Al-4V, Appl. Surf. Sci. 394 (2017) 613–624. https://doi.org/ 10.1016/j.apsusc.2016.10.126.

[11] H.J. Mei, S.S. Zhao, Z.T. Wu, W. Dai, Q.M. Wang, Effect of nitrogen partial pressure on microstructure and mechanical properties of Mo-Cu-V-N composite coatings deposited by HIPIMS, Surf. Coat. Technol. 329 (2017) 68–76. https:// doi.org/10.1016/j.surfcoat.2017.08.041.

[12] H.J. Mei, R. Wang, X. Zhong, W. Dai, Q.M. Wang, Influence of nitrogen partial pressure on microstructure and tribological properties of Mo-Cu-V-N composite coatings with high Cu content, Coatings 8 (2018) 24. https://doi.org/10.3390/ coatings8010024.

[13] G.S. Fox-Rabinovich, K. Yamamoto, M.H. Aguirre, D.G. Cahill, S.C. Veldhuis, A. Biksa, G. Dosbaeva, L.S. Shuster, Multi-functional nano-multilayered AlTiN/ Cu PVD coating for machining of Inconel 718 superalloy, Surf. Coat. Technol. 204 (2010) 2465–2471. https://doi.org/10.1016/j.surfcoat.2010.01.024.

[14] A.D. Pogrebnjak, I.V. Yakushchenko, A.A. Bagdasaryan, O.V. Bondar, R. Krause-Rehberg, G. Abadias, P. Chartier, K. Oyoshi, Y. Takeda, V.M. Beresnev, O.V. Sobol, Microstructure, physical and chemical properties of nanostructured (Ti-Hf-Zr-V-Nb)N coatings under different deposition conditions, Mater. Chem. Phys. 147 (2014) 1079–1091. https://doi.org/10.1016/j.matchemphys.2014.06. 062.

[15] A.D. Pogrebnjak, V.M. Beresnev, K.V. Smyrnova, Ya.O. Kravchenko, P.V. Zukowski, G.G. Bondarenko, The influence of nitrogen pressure on the fabrication of the two-phase superhard nanocomposite (TiZrNbAlYCr)N coatings, Mater. Lett. 211 (2018) 316–318. https://doi.org/10.1016/j.matlet.2017. 09.121.

[16] V. Kouznetsov, K. Macák, J.M. Schneider, U. Helmersson, I. Petrov, A novel pulsed magnetron sputter technique utilizing very high target power densities, Surf. Coat. Technol. 122 (1999) 290–293. https://doi.org/10.1016/S0257-8972 (99)00292-3.

[17] M. Samuelsson, J. Jensen, U. Helmersson, L. Hultman, H. Högberg, ZrB_2 thin films grown by high power impulse magnetron sputtering from a compound target, Thin Solid Films 526 (2012) 163–167. https://doi.org/10.1016/j.tsf.2012. 11.006.

[18] N. Nedfors, A. Mockute, J. Palisaitis, O.Å. Persson, L.Å. Näslund, J. Rosen, Influence of pulse frequency and bias on microstructure and mechanical properties of TiB_2 coatings deposited by high power impulse magnetron sputtering, Surf. Coat. Technol. 304 (2016) 203–210. https://doi.org/10.1016/ j.surfcoat.2016.06.086.

[19] W. Dai, S.H. Kwon, Q.M. Wang, J.M. Liu, Influence of frequency and C_2H_2 flow on growth properties of diamond-like carbon coatings with AlCrSi co-doping deposited using a reactive high power impulse magnetron sputtering, Thin Solid Films 647 (2018) 26–32. https://doi.org/10.1016/j.tsf.2017.12.016.

[20] H.E. Cheng, M.H. Hon, Texture formation in titanium nitride films prepared by chemical vapor deposition, J. Appl. Phys. 79 (1996) 8047–8053. https://doi.org/ 10.1063/1.362358.

[21] S.S. Zhao, H. Du, W.G. Hua, J. Gong, The depth distribution of residual stresses in (Ti,Al)N films: measurement and analysis, J. Mater. Res. 22 (2007) 2659– 2662. https://doi.org/10.1557/JMR.2007.0363.

[22] U. Helmersson, M. Lattemann, J. Bohlmark, A.P. Ehiasarian, J.T. Gudmundsson, Ionized physical vapor deposition (IPVD): A review of technology and applications, Thin Solid Films 513 (2006) 1–24. https://doi.org/10.1016/j.tsf. 2006.03.033.

[23] K. Sarakinos, J. Alami, S. Konstantinidis, High power pulsed magnetron sputtering: A review on scientific and engineering state of the art, Surf. Coat. Technol. 204 (2010) 1661–1684. https://doi.org/10.1016/j.surfcoat.2009.11.013.

[24] F. Papa, H. Gerdes, R. Bandorf, A.P. Ehiasarian, I. Kolev, G. Braeuer, R. Tietema, T. Krug, Deposition rate characteristics for steady state high power impulse magnetron sputtering (HIPIMS) discharges generated with a modulated pulsed power (MPP) generator, Thin Solid Films 520 (2011) 1559–1563. https://doi.org/ 10.1016/j.tsf.2011.09.004.

[25] K. Bobzin, T. Brögelmann, R.H. Brugnara, Aluminum-rich HPPMS $(Cr_{1-x}Al_x)N$ coatings deposited with different target compositions and at various pulse lengths, Vacuum 122 (2015) 201–207. https://doi.org/10.1016/j.vacuum.2015.09.028.

[26] N. Laegreid, G.K. Wehner, Sputtering yields of metals for Ar^+ and Ne^+ ions with energies from 50 to 600 ev, J. Appl. Phys. 32 (1961) 365–369. https://doi.org/ 10.1063/1.1736012.

[27] T. Shimizu, Y. Teranishi, K. Morikawa, H. Komiya, T. Watanabe, H. Nagasaka, M. Yang, Impact of pulse duration in high power impulse magnetron sputtering on the low-temperature growth of wurtzite phase (Ti,Al)N films with high hardness, Thin Solid Films 581 (2015) 39–47. https://doi.org/10.1016/j.tsf. 2014.11.076.

[28] J.A. Hopwood (Ed.), Thin Films: Ionized Physical Vapor Deposition, Academic Press, San Diego CA, 2000, pp. 181–207.

[29] M. Ohring (Ed.), "Materials Science of Thin Films" 2nd Edition, Academic Press, San Diego, New York, 2002, pp. 250–265.

[30] Q. Luo, Characterization of short-range ordered domains using quantitative X-ray diffraction, Nanosci. Nanotech. Let. 10 (2018) 1–9. https://doi.org/10.1166 /nnl.2018.2722.

[31] J.H. Shin, Q.M. Wang, K.H. Kim, Microstructural evolution and tribological behavior of Mo-Cu-N coatings as a function of Cu content, Mater. Chem. Phys. 130 (2011) 870–879.

[32] H. Zhou, J. Zheng, B. Gui, D. Geng, Q. Wang, AlTiCrN coatings deposited by hybrid HIPIMS/DC magnetron co-sputtering, Vacuum 136 (2017) 129–136. https: //doi.org/10.1016/j.vacuum.2016.11.021.
[33] J. Pelleg, L.Z. Zevin, S. Lungo, Reactive-sputter-deposited TiN films on glass substrates, Thin Solid Films 197 (1991) 117–128. https://doi.org/10.1016/0040- 6090(91)90225-M.
[34] G.Abadias, Stress and preferred orientation in nitride-based PVD coatings, Surf. Coat. Technol. 202 (2008) 2223–2235. https://doi.org/10.1016/j.surfcoat.2007. 08.029.
[35] A.J. Perry, V. Valvoda, D. Rafaja, On the residual stress and picostructure of titanium nitride films–II. A picostructural model, Vacuum 45 (1994) 11–14. https://doi.org/10.1016/0042-207X(94)90332-8.
[36] Z.T. Wu, P. Sun, Z.B. Qi, B.B. Wei, Z.C. Wang, High temperature oxidation behavior and wear resistance of $Ti_{0.53}Al_{0.47}N$ coating by cathodic arc evaporation, Vacuum 135 (2017) 34–43. https://doi.org/10.1016/j.vacuum.2016.10.030.
[37] C.W. Kim, K.H. Kim, Anti-oxidation properties of TiAlN film prepared by plasma-assisted chemical vapor deposition and roles of Al, Thin Solid Films 307 (1997) 113–119. https://doi.org/10.1016/S0040-6090(97)00212-5.
[38] C.L. Chang, S.G. Shih, P.H. Chen, W.C. Chen, C.T. Ho, W.Y. Wu, Effect of duty cycles on the deposition and characteristics of high power impulse magnetron sputtering deposited TiN thin films, Surf. Coat. Technol. 259 (2014) 232–237. https://doi.org/10.1016/j.surfcoat.2014.03.011.
[39] J.A. Thornton, Influence of apparatus geometry and deposition conditions on the structure and topography of thick sputtered coatings, J. Vac. Sci. Technol. 11 (1974) 666–670. https://doi.org/10.1116/1.1312732.
[40] Q. Luo, D.B. Lewis, P.E. Hovsepian, W.D. Münz, Transmission electron microscopy and X-ray diffraction investigation of the microstructure of nanoscale multilayer TiAlN/VN grown by unbalanced magnetron deposition, J. Mater. Res. 19 (2004) 1093–1103. https://doi.org/10.1557/JMR.2004.0143.
[41] P. Yashar, S.A. Barnett, J. Rechner, W.D. Sproul, Structure and mechanical properties of polycrystalline CrN/TiN superlattices, J. Vac. Sci. Technol. A 16 (1998) 2913–2918. https://doi.org/10.1116/1.581439.
[42] K.E. Pappacena, D. Singh, O.O. Ajayi, J.L. Routbort, O.L. Erilymaz, N.G. Demas, G. Chen, Residual stresses, interfacial adhesion and tribological properties of MoN/Cu composite coatings, Wear 278 (2012) 62–70. https:// doi.org/10.1016/j.wear.2012.01.007.
[43] N. Bagcivan, K. Bobzin, G. Grundmeier, M. Wiesing, O. Ozcan, C. Kunze, R.H. Brugnara, Influence of HPPMS pulse length and inert gas mixture on the properties of (Cr,Al)N coatings, Thin Solid Films 549 (2013) 192–198. https:// doi.org/10.1016/j.tsf.2013.06.036.
[44] P. Zeman, R. Čerstvý, P.H. Mayrhofer, C. Mitterter, J. Musil, Structure and properties of hard and superhard Zr-Cu-N nanocomposite coatings, Mater. Sci. Eng. A 289 (2000) 189–197. https://doi.org/10.1016/S0921-5093(00)00917-5.
[45] D.C. Tsai, Z.C. Chang, B.H. Kuo, C.T. Tsao, E.C. Chen, F.S. Shieu, Influence of discharge power on the structural, electro-optical, and mechanical properties of (TiZrHf)N coatings, J. Alloy. Compd. 622 (2015) 446–457. https://doi.org/ 10.1016/j.jallcom.2014.10.073.
[46] Y.X. Ou, J. Lin, S. Tong, H.L. Che, W.D. Sproul, M.K. Lei, Wear and corrosion resistance of CrN/TiN superlattice coatings deposited by a combined deep oscillation magnetron sputtering and pulsed dc magnetron sputtering, Appl. Surf. Sci. 351 (2015) 332–343. https://doi.org/10.1016/j.apsusc.2015.05.110
[47] H.J. Mei, S.S. Zhao, Q.M. Wang, Residual stress of TiN multilayer coatings alternately deposited by arc ion plating and magnetron sputtering, Nanosci. Nanotech. Let. 9 (2017) 885–891. https://doi.org/10.1166/nnl.2017.2393.